Open Journal of Nano
ISSN: 2147-0081
(2025) 10–1&2
Research Article

Ferrite-Based Hierarchical Nanostructures for Electrochemical Sensing: Synthesis, Interface Engineering, and Performance Insights

[1]Iqra Khalid, [2]Abdullah Faheem, [*1]**Akbar Ali**

[1] COMSATS University Islamabad-Lahore Campus, Depart. of Physics, Lahore, Pakistan.
[2] SICAS Liberty Campus, Lahore, Pakistan.
* Corresponding Author, e-mail: drakbar.ali@cuilahore.edu.pk

Submission Date: 14.09.2025 Acceptation Date: 21.11.2025

Abstract - A non-enzymatic choline biosensor was demonstrated with chitosan (CS) supported $NiFe_2O_4$ modified on a carbon paste electrode (CPE). $NiFe_2O_4$ is synthesized via the hydrothermal method to study the choline chloride (ChCl) behavior towards the distinctive performance of choline. The prepared sample with CPE. The synthesized $NiFe_2O_4$ was examined with different characterization techniques to confirm the formation of the specified material. X-ray diffraction (XRD), Fourier-Transmission Infrared spectroscopy (FTIR), and Raman Spectroscopy were used to optimize and evaluate the various properties of the prepared material. XRD confirmed the cubic inverse spinel crystal structure of $NiFe_2O_4$ with a crystallite size of 14nm, while FTIR spectra revealed the stretching and bending vibration over the IR frequency range, and modes confirmed through Raman spectra frequency range. The modified electrode of $NiFe_2O_4$/CS/CPE was used to perform electrochemical studies by voltammogram and evaluated through Cyclic voltammetry (CV). The CV curves taken at different working ranges (5-15µL) of potential 0.0- +1.0 V and the analyte signal of LoD (0.002µM), considering the S/N=3 across the current system, with the linear regression (R^2) of 0.99. The prepared electrode showed a low (LoD) in the smaller range of the chloride choline and demonstrated a good response.

Keywords: Nanocomposites, Ferrites Nanomaterials, Electrochemical Sensor, Biosensor

GRAPHICAL ABSTRACT

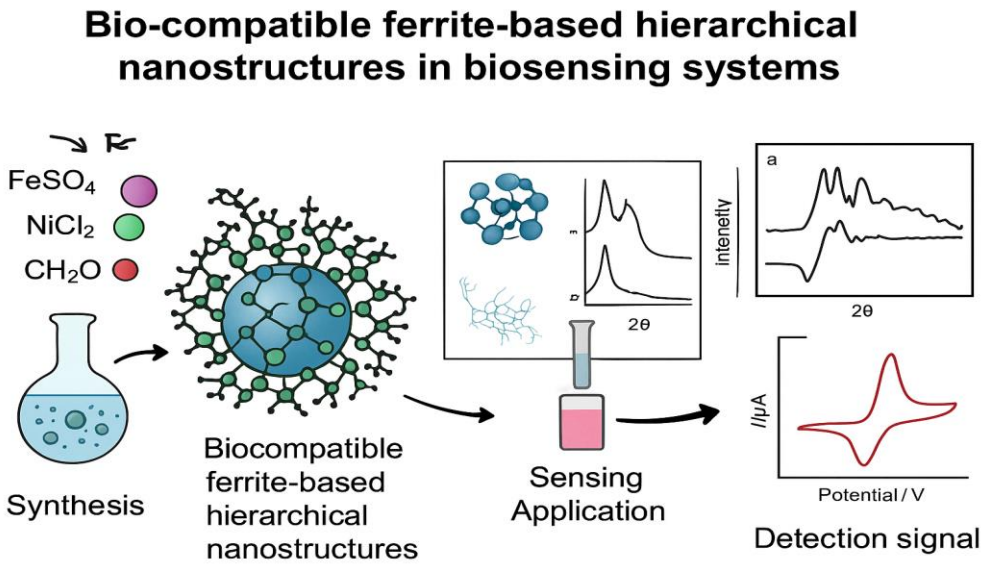

DOI: 10.56171/ojn.1778109

Open Journal of Nano
ISSN: 2147-0081
(2025) 10–1&2
Research Article

1. Introduction

Nickel ferrite is one of the most attractive nanostructure materials, having an equal distribution of tetrahedral and octahedral sites and containing inverse spinel shows great properties as an electrode material. $NiFe_2O_4$ and its nanostructure are good candidates that exhibit large thermal and chemical stability, show excellent electrochemical behavior and their applicable in different fields as energy storage devices, large density recording value and biomedicine. The nanocomposites of $NiFe_2O_4$ as a cathode material are highly effective and show great stability, selectivity, linearity and detect rapid dopamine, uric acid and ascorbic acid in real samples [1,2]. Chitosan-based nickel ferrite nanoparticles form high-performance films, good biocompatibility, and high mechanical strength, performing as highly compatible biosensors and called polymer-based biosensors [3,4]. They have a wide space in the emergence of new well-structured biomaterials and determine the biotic immune assay, detection of an analyte in real and clinical samples and the quantity of particles in drug delivery [5]. Nickel ferrite nanoparticles based on chitosan show excellent performance for biosensing of choline, as the structure of $NiFe_2O_4$ is shown in Figure 1.

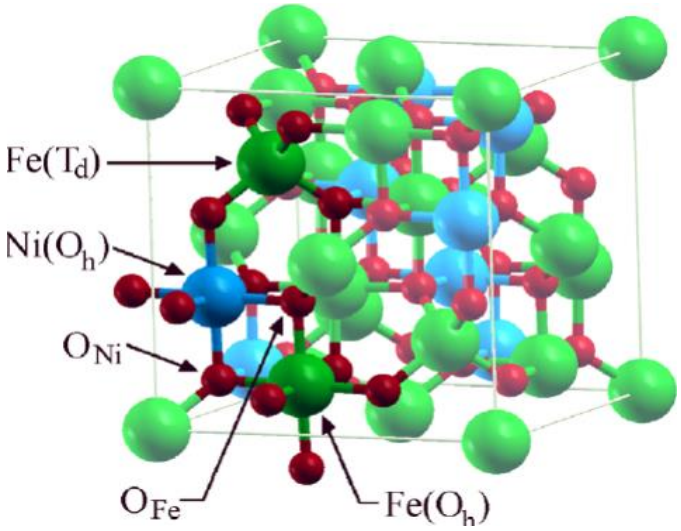

Figure 1. Crystal structure of inverse spinel $NiFe_2O_4$

Choline or $C_5H_{14}NO^+$(trimethyl-beta-hydroxyethyl-ammonium) is an essential nutrient. It acts as a precursor for the biosynthesis of many neurotransmitters, such as acetylcholine. Choline's deficiency and its abnormal metabolism can cause neurodegenerative disorders, liver dysfunction and multiple cancers [6,7]. Choline, an important source of initial upgrading of brain cells, is needed at an early age in the diet because it influences neural tube closure, apoptotic messaging in neurons and liver cells and hepatic transport of lipoproteins. Alpha-glycerophosphocholine (GPC) is another name for choline alfoscerate ($C_8H_{20}NO_6P$), a cholinergic molecule and precursor to ACh that is widely used as a dietary supplement. The dose of choline under the recommendation of the department concerned for adults must be greater than 550mg/day, and we can take it under regular use of enriched foods having a concentration of choline for metabolism. So, monitoring the level of choline in serum through the proper channel, providing a good electrochemical response, is very important [8,9]. Choline metabolism, with its relevant characteristics, is shown in Figure 2.

DOI: 10.56171/ojn.1778109

Open Journal of Nano
ISSN: 2147-0081
(2025) 10–1&2
Research Article

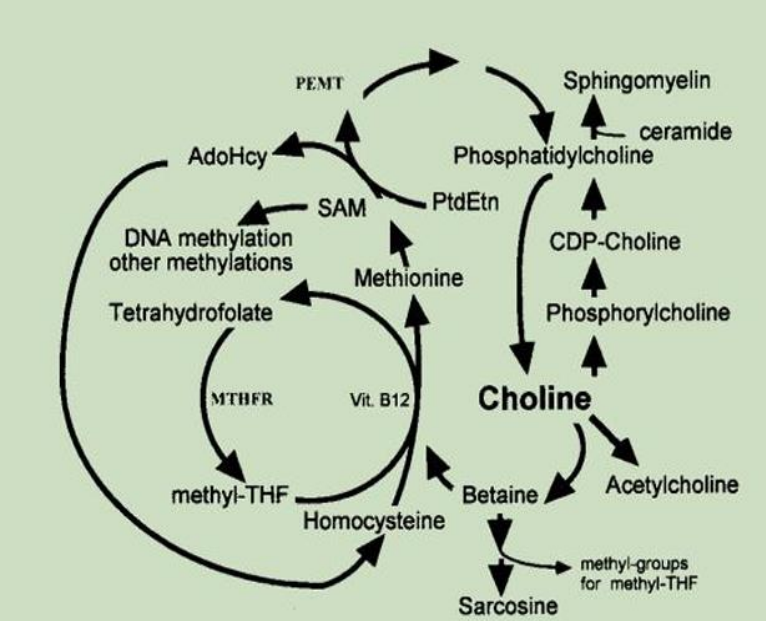

Figure 2. Choline's metabolism, its components, and related nutrients

The non-enzymatic choline's sensing can be achieved by using choline as an analyte and the oxidation of the neurotransmitter performs the electrocatalytic properties. Electrochemical performance was checked with the rate of limit of detection, the linear range and sensitivity and calculated by using different techniques. The range for non-enzymatic choline sensors varied from 0.05 to 10.0 (mM), the limit of detection (LOD) is from (-134 to 25.4) μM or (-97 to 60.5) $\mu AmM^{-1}cm^{-2}$ by going through different transition metals literature [10]. Electrochemical biosensors are the most promising tool that provides economical, quick and specific biomolecule sensing channels with an excellent response time, durability and selectivity and are classified according to their transduction mechanism [11]. The extraction and/or hydrolysis method is the primary hurdle in the analysis of choline in consumed foods and dietary supplements. New studies of non-enzymatic chemical sensors have used metals and metal oxides as sensing materials. These materials demand strong alkaline solutions, such NaOH and KOH, and high synthesis temperatures to detect acetylcholine as a direct measure of choline. Potentiometric sensors, which rely on the measurement of electrical potential and generate a change in potential according to the logarithm of the activity of the ion of interest in the sample, can be designed enzyme-free because choline is a cation [12–14].

Biosensors are devices that recognize a biological material based on the integration of self-made receptors and transducers, which are very close to electrochemical transducers. These electrochemical sensors display the intrinsic selectivity and particularity of the receptor, joined with the large value of stability and low recognition limit of the analyte. They can be formed with miniaturization and efficiently manufactured for a minimal price and furnish a quick logical reaction with a couple of micro-liters of test [15,16]. The modern sensor devices consist of the insertion of new nanostructures, which are used to enhance the identification of the analyte, referred to as sensitivity, lower limit of detection (LOD), and specificity [17,18]. As compared to previously reported electrodes, the electrochemical sensors that were doped using various nanomaterials showed better sensitivity and selectivity for choline detection. In addition to increasing response signal sensitivity, the doped Fe_3O_4 magnetic nanoparticles with other materials utilised as peroxidase mimics in the choline biosensor have advantageous features of stability, magnetic separation, and relatively simple fabrication [7,19]. Moreover, materials like nano-gold, magnetic nanoparticles, silver nanorods, lanthanide-doped nanoparticles, and heterogeneous nanowires were included in the nanosensors employed in these applications. Recent advancements have influenced the selection criterion for MIONPs for biomedical applications thus far. Magnetic iron oxide nanoparticles (MIONPs) that are optimized should: i. have the right size and desired magnetic properties; ii. be

DOI: 10.56171/ojn.1778109

Open Journal of Nano
ISSN: 2147-0081
(2025) 10–1&2
Research Article

uniform in size and shape to guarantee repeatable performance; iii. minimize surface disorders and crystallographic defects to maximize magnetic properties; and iv. appropriate surface functionalities that guarantee colloidal stability and biocompatibility in physiological environments [20,21]. Herein, we report the synthesis of $NiFe_2O_4$ via the hydrothermal method and further modified a carbon paste electrode (CPE) with the $NiFe_2O_4$/CS process for the choline chloride quantification, which is the first time that work has been done on it. The distinctive structure of $NiFe_2O_4$/CS composites offers excellent stability and linear regression, and it also ensures stable performance of the blended electrode with choline chloride. In the second half of the work, different characterization techniques were discussed to confirm the structural properties, vibrational modes, size distribution, and electrochemical behavior of $NiFe_2O_4$/CS.

2. Materials and Methods

Ferric chloride hexahydrate ($FeCl_3.6H_2O$) and nickel Chloride hexahydrate ($NiCl_2.6H_2O$) were purchased from Merck Sigma, USA. NaOH (25% solution) was sourced from Thermo Fisher Scientific (UK). For the preparation of $NiFe_2O_4$/CS modified CPE, Chitosan (CS) of low molecular weight and Choline chloride (ChCl) $[CH_3)_3NCH_2CH_2OH]$ Cl, were purchased from Sigma-Aldrich. A carbon paste electrode (CPE) of 0.5mm thickness was used in this research work. Further, deionized water was used throughout the experimentation.

2.1. Synthesis of $NiFe_2O_4$ Nanoparticles

The $NiFe_2O_4$ was prepared via the hydrothermal method. To prepare the solution of chlorides, 40 ml of deionized (DI) water was taken in different-sized beakers for each salt precursor and stirred on the magnetic hot plate until it became homogeneous. Then, we obtained the homogeneous mixture of both the salts after 1 hour of stirring. 1M solution of sodium hydroxide was added dropwise into the solution until the pH~11 of the solution was maintained and stirred constantly. After the addition of NaOH, the metal chlorides will be precipitated into a dark brown color, containing metal hydroxide of the form Fe $(OH)_3$ and Ni $(OH)_2$, respectively. Then the solution was autoclaved and placed into an oven at 200 ^oC for 15 hours. The particles were collected according to their density after washing 15 to 20 times with DI water under centrifugal force. Then, the collected liquid form was placed into an oven at 90 ^oC for 8-9 h to obtain a completely dry sample. The grinding of the sample was performed to get a fine powder with great homogeneity and to reduce the particle size. The grinding process of the sample was done by using a pestle and mortar. The sample has been saved in the bullet box for further processing [22].

2.2. Modification of the electrode with the synthesized $NiFe_2O_4$ based on chitosan (CS)

The carbon paste electrode (CPE) substrate of HB (0.5mm) was used after cleaning and washing with deionized water. The carbon paste electrode has been modified by using synthesized NiFe2O4 powder composite with chitosan. Firstly, the PBS buffer was prepared by taking 5 tablets of phosphate buffer saline in 500 mL of distilled water and setting aside until we got a homogeneous solution. The slurry of NiFe2O4/CS was prepared in the PBS buffer at room temperature. The measured quantity of NiFe2O4 powder (5mg) and chitosan (3mg) was mixed into an 8µL solution of PBS and placed into a sonication bath for 40 min. The washed bare carbon paste electrode of small thickness is taken and put into the prepared slurry for 20 min and set aside at 25 °C. The freshly prepared electrode was used as a working electrode for the non-enzymatic quantification of choline based on a three-electrode system. The analyte for the detection of biomarkers was prepared by taking a quantity of chloride about 0.28 g, put into a 1mM solution of PBS and all the steps proceeded under pH ~ 7 at room temperature. The analyte is ultrasonicated for 30 min and used as prepared. The second step includes the preparation of an analyte for the detection of biomarkers. The measured quantity of choline is about 0.28 g, put into a 1mM solution of PBS and all the steps proceed under pH ~ 7 at room temperature. The analyte is ultrasonicated for 30 min and used as prepared.

DOI: 10.56171/ojn.1778109

Open Journal of Nano
ISSN: 2147-0081
(2025) 10–1&2
Research Article

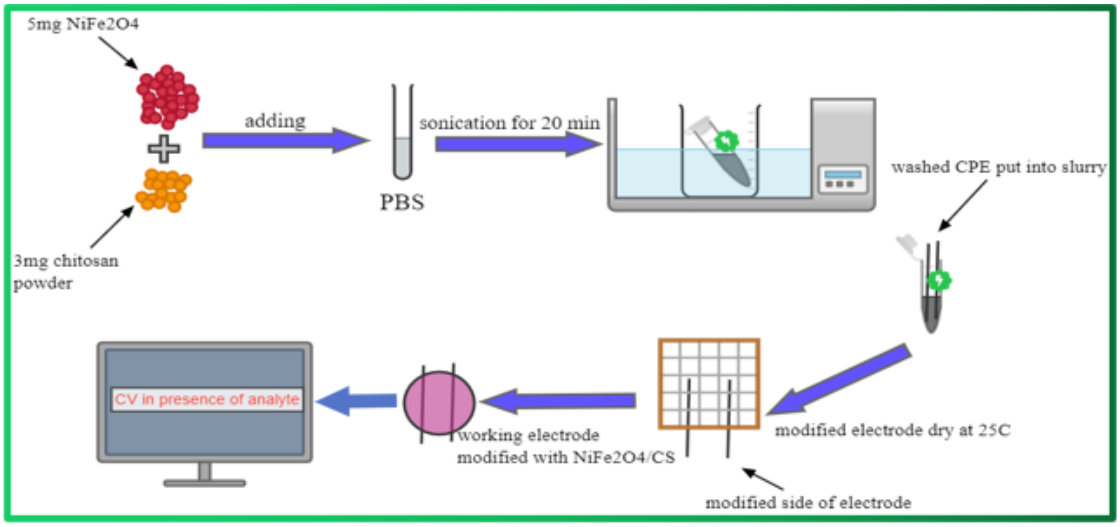

Figure 3. Schematic representation for the preparation of $NiFe_2O_4$/CS modified CPE

3. Results and Discussions

XRD analysis was done using an X-ray diffractometer (Perkin Elmer Diamond Series) with Cu-Ka radiation source (k = 1.5406 A˚) to examine the crystal structure of NiFe2O4 materials and structural parameters calculated subsequently. Figure 4a illustrates the XRD spectroscopy measurements of the NiFe2O4 synthesized via the hydrothermal method. The results from the XRD data using wavelength λ = 0.15406 nm and a radiation source of CuKα have been investigated for the various structural parameters at different peak values. The indexed pattern represents the crystal planes (220), (311), (222), (400), (422), and (511) formed by following Bragg's law, βins = 0.573o matched with the reference pattern: NiFe2O4, 96-591-0065 [23]. The prepared sample has a cubic inverse spinel structure, and there are no impurity peaks found in the boundary of X-ray detection. The XRD analysis of NiFe2O4 represents the single-phase structure. The intense and sharp peaks are an indication of good crystallinity of NiFe2O4, and the crystallite size (D) was calculated by using Scherrer's formula $\boldsymbol{D = \frac{0.9\lambda}{\beta cos\theta}}$. The prepared sample has a cubic inverse spinel structure, and no impurity peaks are found in the X-ray detection boundary. The XRD analysis of NiFe2O4 represents the single-phase structure. The lattice constant (a) is calculated from the interplanar spacing (d) value by using the relation:

$$a = d\sqrt{h^2 + k^2 + l^2}$$

Where (hkl) represent the Miller indices, and the value of "d" has been calculated for all the planes indexed at sharp intensity values defined in Table 1.

Table 1. Calculated values of different parameters from the XRD pattern with 2% Ni.

Sr. no	Angle 2θ (º)	Miller indices (*h,k,l*)	Inter-planer Spacing d (Å)
1.	30.34º	220	2.95
2.	35.74º	311	2.88
3.	43.39º	400	2.94
4.	53.80º	402	2.79
5.	57.37º	511	2.93

The crystallite size (D) and microstrain (ε) = β have been calculated by using line broadening values (β) and the small average crystallite size (D) calculated to be 14nm, indicating that an ultra-fine NiFe2O4 formed, while the broad peaks have a large FWHM, providing a small value of crystallite size. The dislocation density (δ) = 1/D2 is also calculated from data points of D shown in

DOI: 10.56171/ojn.1778109

Open Journal of Nano
ISSN: 2147-0081
(2025) 10–1&2
Research Article

Table 2. The distortion in the crystal structure and some imperfections refer to the strain due to the peak's broadening [24].

Table 2. Calculation of FWHM, crystallite size (D), microstrain (ε), and dislocation density (δ).

Sr. no	Angle (θ)	FWHM (radians)	Crystallite size D (nm)	Microstrain (ε)	Dislocation Density δ×10-2 (nm-2)
1.	15.17o	0.58	14	0.91	0.39
2.	17.87o	0.52	15	0.91	0.39
3.	21.69o	0.58	13	0.90	0.40
4.	26.9o	0.57	16	0.89	0.40
5.	28.68o	0.58	12	0.90	0.39

Where β represents the full width half maxima (FWHM) and relates to line broadening, half of the detection angle (θ), called Bragg's angle, λ is the X-ray wavelength, and 0.9 is Scherrer's constant (k) within the limit of Gauss's formula [25]. The crystal data collected for the cubic spinel structure have a chemical formula Ni16.00Fe8.00O32.00, which forms the space group Fd-3m, density of 580.09g/cm3 with lattice parameter (a) = 8.34Å. The small average crystallite size (D) calculated at 14nm indicates that an ultra-fine NiFe2O4 formed, while the broad peaks have a large FWHM, providing a small value of crystallite size. The distortion in the crystal structure and some imperfections refer to the strain due to the peak's broadening [26,27]. The XRD pattern of NiFe2O4 with a smaller concentration of nickel salt is shown in Figure 4b. The precursor of the sample was prepared through a hydrothermal method, and the intense peaks involved the angles 2θ = 35.5o, 43.1o, 53.9o and 57.1°, showing the cubic and face-centered type of NiFe2O4 matched with the reference pattern: NiFe2O4, 96-591-0065 through Xpert High Score Plus, as shown in Table 3. The other peaks representing the presence of hydroxide and observed at high intensity referred to another phase and were present due to the large concentration of sodium hydroxide, which is used in this sample during the experimental procedure of NiFe2O4 formation [28]. The crystal data collected for the cubic structure have a chemical formula Ni16.00Fe8.00O32.00, which forms the space group Fd-3m, density of 580.09g/cm3, with lattice parameter (a) = 8.34 Å.

Table 3. Calculated values of different parameters from the XRD pattern with 4% Ni.

Sr. no	Angle 2θ°	Miller indices (*h,k,l*)	Inter-planer Spacing d (Å)
1.	35.58°	311	2.52
2.	43.74°	400	2.52
3.	53.97°	402	2.58
4.	57.42°	511	2.59

The data points have been mentioned at various intensities with 2θ values in Table 4. and the crystallite size (D) has also been determined against Miller indices (h,k,l) by the FWHM value shown in Table 4. The calculated range of microstrain has decreased as the peaks became sharper and the FWHM of the defined peaks reduced. The peak around 33.3o is attributed to higher water oxidation and the formation of oxide occurs at this angle [29]. The average crystallite size (D) calculated is 32 nm for the mentioned peaks.

Table 4. Calculation of FWHM, crystallite size (D), microstrain (ε) and dislocation density (δ).

Sr. no	Angle (θ)	FWHM (radians)	Crystallite size D (nm)	Microstrain (ε)	Dislocation Density δ×10^{-2} (nm^{-2})
1.	17.81°	0.16	36	0.20	0.026
2.	21.86°	0.16	34	0.19	0.023
3.	26.98°	0.16	30	0.18	0.030
4.	28.78°	0.21	28	0.17	0.045

DOI: 10.56171/ojn.1778109

Open Journal of Nano
ISSN: 2147-0081
(2025) 10–1&2
Research Article

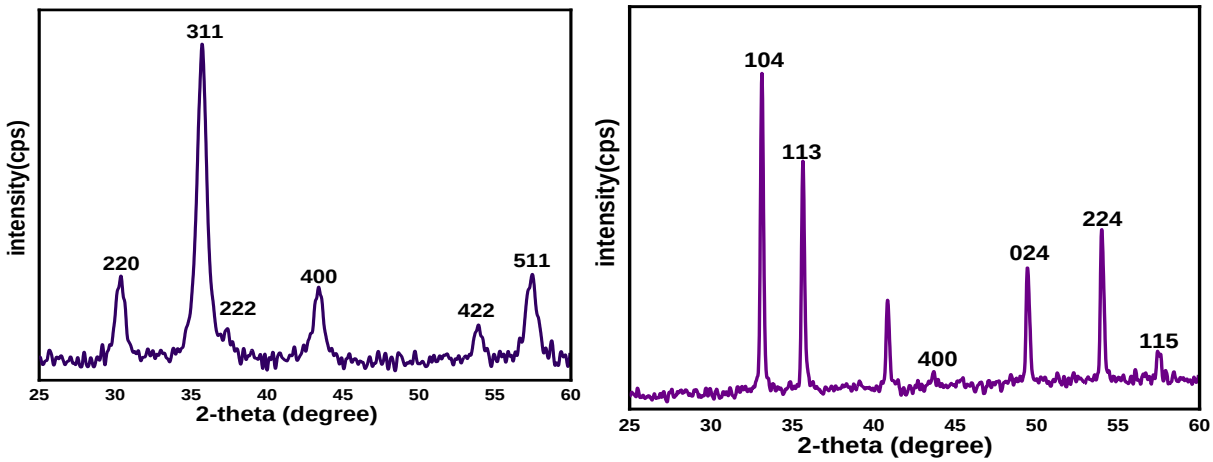

Figure 4. (a) XRD pattern peaks of $NiFe_2O_4$ 2%, (b) 4% Ni-concentration.

Raman analysis was done using a Raman Microscope (RENISHAW UK) with the excitation laser 514nm and laser exposure time of 10s, having laser power 50%. In the present study, the NiFe2O4 spectra exhibit several bands and intensity of the dehydrated material across the applied wavelength, as shown in Figure 5. The NiFe2O4 spectroscopy studies the characteristic bands having 5 Raman active modes A1g, 3T2g, and Eg, while the strong and broadened peaks around 464cm-1 and 699cm-1 have a connection with the crystallized spinel structure of NiFe2O4. These sharp valued peaks are the allocation to octahedral and tetrahedral sites of Fe+3 and Ni+2 on the sites of the crystal structure. The peak values oriented at 213cm-1 and 279cm-1 represent the dispersion bands of NiFe2O4 powder, and the band (T2g) at 497cm-1 is formed due to the peak's allotment around 490cm-1 and 522cm-1, as shown in Figure 5. The difference in peaks around 200-400 cm-1 occurs due to the varied ionic radii of Ni and Fe ions, and A1g mode at 497cm-1 formed the Fe2O3-hematite. All the bands at peak values of 213, 279, 358, 497, 539, 522, and 699cm−1 represent the symmetrical and anti-symmetrical stretching of an oxygen atom at the octahedral and tetrahedral sites. The composition of nickel with iron has an impact on the crystal structure of the formed nanoparticles; a higher percentage of nickel and a large reaction temperature have resulted in a sharp and intense peak of inverse spinel nickel ferrite. The ferrite's inverse spinel structure has more intense peaks at the band values 464cm-1 and 497 cm-1, owing to high temperature, and shifted towards higher frequency as shown below at 699cm-1. They contribute to the vibration modes formed due to oxygen atoms, remark to Fe3+ and (Fe3+ and Ni2+) octahedral and tetrahedral sites [30]. The weak and less intense peaks at 530cm-1 correlate with the transfer of nickel ions from the octahedral site to the tetrahedral site and result in a highly cation-disordered disorder. The wider and intense peaks from 630cm-1 to 699cm-1 in all the Raman spectra graphs given below represent the Eg phonon mode and A1g (tetrahedral breathing mode) with the formation of a tetrahedron in ferrites. The T2g modes at a large peak of 213cm-1 represent the single crystal structure of NiFe2O4, and these bands formed because of the low heat treatment, as shown in Figure 5 [31].

DOI: 10.56171/ojn.1778109

Open Journal of Nano
ISSN: 2147-0081
(2025) 10–1&2
Research Article

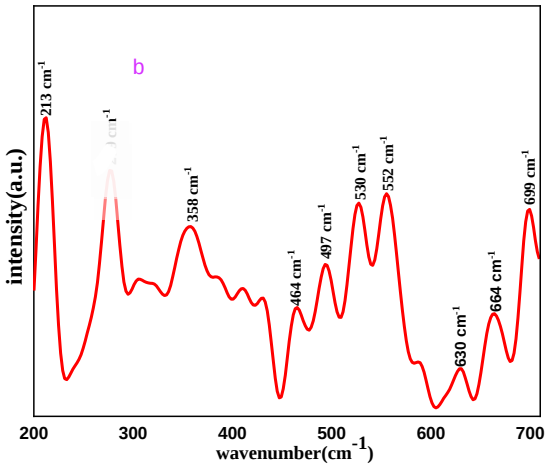

Figure 5. Raman spectra correspond to $NiFe_2O_4$ nanoparticles. Formation of $NiFe_2O_4$ as synthesized with the molar ratio 1:2.

FTIR studies are done by a Varian-4100 spectroscope. Figure 6. shows the FTIR absorbance spectra of the synthesized NiFe2O4 in the wavenumber range of 500-4000cm-1. The selected range of frequency for the absorbance spectra of nickel ferrite elaborates the stretching and bending vibrations of the different functional groups. The peak values at 648cm-1, 896cm-1, and 1652cm-1 are due to the stretching and bending vibration of the C-N=O, C-C, and C=O. The peak value at 648cm-1 is attributed to the tetrahedral inverse spinel structure of NiFe2O4, and the other lower peak frequency value at 896cm-1 and 1652cm-1 subsists the stretching vibration of α-FeOOH, deformation and bending vibration of -OH in ϒ-FeOOH. The formed bands are at different positions because of the radii difference of Fe-O in the inverse spinel A and B sites [32–34]. The existence of the iron oxide around 1000cm-1 or less, favorably observed for vibrations, atomic levels of the material, and the stretching vibration, is the framework of the octahedral vibration [35]. The IR active molecules with the different functional groups at 896cm-1 and 2181cm-1 are preferable to C=C and the absorbance of CO2 from the air. While the frequency mode of high peak value at 3318cm-1 indicates the presence of (OH) hydroxyl group, concerned with the hydrogen-bonded stretching vibration [36,37].

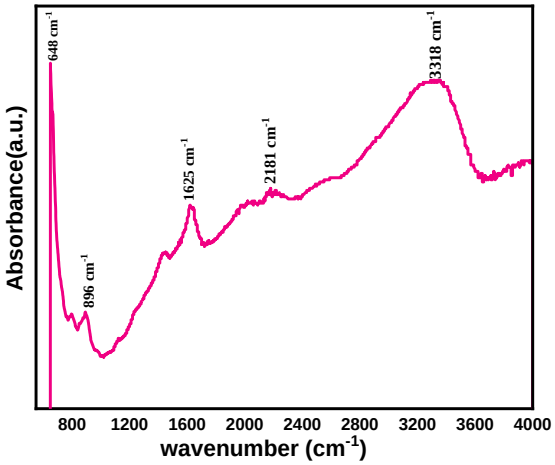

Figure 6. FTIR measured spectra of $NiFe_2O_4$ (1:2).

3.1. Electrochemical Analysis Cyclic Voltammetry (CV)

The graphite paste electrode modified NiFe2O4/CS is held for electrochemical performance without analyte and with 1mM choline (choline chloride) in 20mM PBS using cyclic voltammetry (CV) at 100 mVs-1 scan rates. The bare GCE without modification showed no oxidation, while the peak current increased for NiFe2O4/CS modified CPE, as shown in Figure 7 (a). Choline oxidation

DOI: 10.56171/ojn.1778109

Open Journal of Nano
ISSN: 2147-0081
(2025) 10–1&2
Research Article

is described by varying the concentration of choline and showing that the modified electrocatalyst oxidizes the choline, as shown in Figure 7 (b). The other interface and biomolecule also contributed to the detection of choline and disturbed the anodic peak current (Ip). The anodic current of the modified electrode increased in the selected range of choline concentration from 0.005 to 0.015 mM. The plot of modified electrodes at different concentrations has been taken using a Pt-wire as a counter electrode, which provides the resultant current. The scanned potential over the modified electrode transfers the electron, and the choline is oxidized at +0.5 V. The cathodic current increased directly with the analyte range, and a large concentration of choline chloride showed maximum oxidation for the modified electrode compared to the blank electrode, and for the modified electrode detected without choline. The linear curve manipulates the various concentrations of choline chloride (0.005 mM, 0.010 mM & 0.015 mM). The modified electrode showed a limit of detection (LoD) of 0.002 µM or limit of quantification (LoQ) of 0.0086 µM, which was measured through a linear calibration function having a regression coefficient (R2) of 0.99 over the applied working range, as shown in Figure 8 [38].

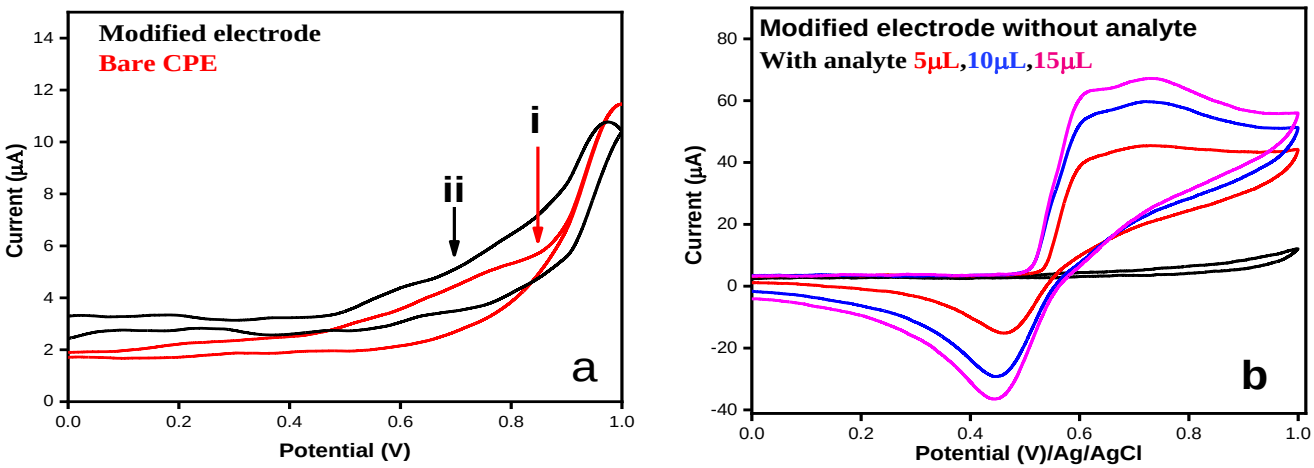

Figure 7. Cyclic voltammograms of $NiFe_2O_4$/CS/CPE (a) i: bare CPE ii: $NiFe_2O_4$/CS modified CPE (b) CV curves supporting electrolyte PBS 0.02 mM, analyte 1mM; scan rate 100 mVs^{-1} of $NiFe_2O_4$/CS modified CPE with the choline chloride working limit (5µL-15µL).

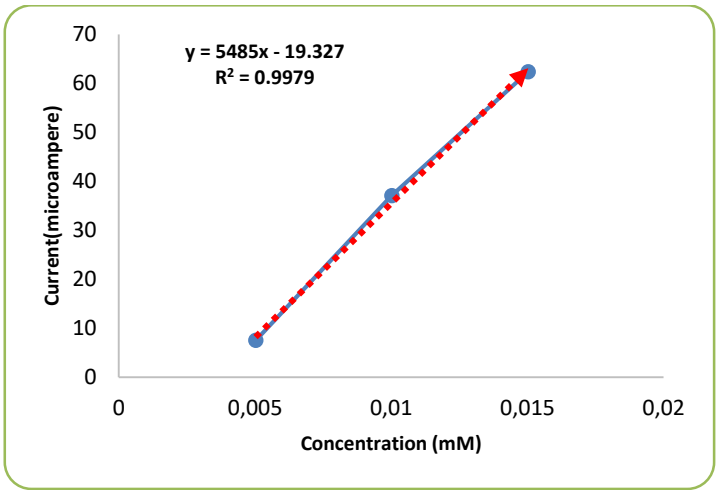

Figure 8. Calibration graph artifacts the analyte sensitivity (ChCl) into the linear range of (0.005mM-0.015mM) at 25ºC quantified over a small range.

DOI: 10.56171/ojn.1778109

4. Conclusions

In this study, the choline detection has been discussed using the synthesized CS based $NiFe_2O_4$ modified with GCE. The prepared material has good electrochemical behavior towards advances in choline biosensing with simple step analysis. The prepared sample of $NiFe_2O_4$ showed the cubic inverse spinel structure and crystalline nature, having a crystallite size of 14nm with a lattice parameter of 0.84nm. The average particle size of the samples was calculated as 14nm, 25nm, and 37nm. The FTIR spectra analyzed the octahedral and tetrahedral stretching vibration at 471cm^{-1} and 648cm^{-1}. The inverse spinel A and B sites are formed at different positions because of the radii difference of Fe-O and Ni. The Raman Spectra with the 5-Raman active modes (A_{1g}, $3T_{2g,}$ and E_g) confirmed and, at a frequency of 699 cm^{-1}, justified A_{1g} (tetrahedral breathing mode) and referred to the tetrahedral sites of Ni^{+2} on the B site of the crystal structure. The modified electrode for choline quantification has been discussed with CV and cyclic voltammogram at the smallest linear range of choline chloride (0.005 mM-0.015 mM) defines the mechanism of electrocatalysis of choline with the lowest limit of detection (LLoD) of 0.002 µM. The modified electrode showed the large oxidation of choline on their surface at the fixed potential of reference electrode in the presence of choline chloride as compared to without choline chloride (ChCl)curves of bare and modified electrode.

Peer-review: Externally peer - reviewed.

Author contributions: Author A, B: Writing – review & editing, Writing – original draft, Visualization, Formal analysis, Data curation. Author C: Formal analysis, Writing – review & editing.

Conflict of Interest: No conflict of interest was declared by the authors.

Financial Disclosure: We are thankful to the Higher Education Commission of Pakistan for the grant of this project (NPRU-15417) titled ‘Ternary nano biocomposites for the fabrication of a novel electrode for the detection of chemical biomarkers,’ and to the Department of Physics, COMSATS University Islamabad, for its support in this research work.

References

[1] T. Ost Fracari, N.H. Lazzari, J. Chaves Ortiz, J. Arguello, V. Lavayen, Nickel ferrite nanoparticles on a carbonaceous matrix and their colorimetric assay for ascorbic acid detection, React. Kinet. Mech. Catal. 130 (2020) 463–476. https://doi.org/10.1007/s11144-020-01780-1.

[2] R. Madhuvilakku, S. Piraman, One-dimensional NiFe2O4 nanorods modified with sulfur-rich spherical carbon nanoparticles for simultaneous voltammetric determination of ascorbic acid, dopamine and uric acid, Microchim. Acta 186 (2019) 434. https://doi.org/10.1007/s00604-019-3496-4.

[3] H.Q. Alijani, S. Pourseyedi, M. Torkzadeh-Mahani, A. Seifalian, M. Khatami, Bimetallic nickel-ferrite nanorod particles: greener synthesis using rosemary and its biomedical efficiency, Artif. Cells Nanomedicine Biotechnol. 48 (2020) 242–251. https://doi.org/10.1080/21691401.2019.1699830.

[4] F. Yalçıner, E. Çevik, M. Şenel, A. Baykal, Development of an Amperometric Hydrogen Peroxide Biosensor based on the Immobilization of Horseradish Peroxidase onto Nickel Ferrite Nanoparticle-Chitosan Composite, Nano-Micro Lett. 3 (2011) 91–98. https://doi.org/10.1007/BF03353657.

[5] M.K. Shobana, Nanoferrites in biosensors – A review, Mater. Sci. Eng. B 272 (2021) 115344. https://doi.org/10.1016/j.mseb.2021.115344.

[6] P. Rahimi, Y. Joseph, Enzyme-based biosensors for choline analysis: A review, TrAC Trends Anal. Chem. 110 (2019) 367–374. https://doi.org/10.1016/j.trac.2018.11.035.

[7] Z. Zhang, X. Wang, X. Yang, A sensitive choline biosensor using Fe3O4 magnetic nanoparticles as peroxidase mimics, The Analyst 136 (2011) 4960. https://doi.org/10.1039/c1an15602k.

[8] U. Kansakar, V. Trimarco, P. Mone, F. Varzideh, A. Lombardi, G. Santulli, Choline supplements: An update, Front. Endocrinol. 14 (2023) 1148166. https://doi.org/10.3389/fendo.2023.1148166.

[9] S. Pundir, N. Chauhan, J. Narang, C.S. Pundir, Amperometric choline biosensor based on multiwalled carbon nanotubes/zirconium oxide nanoparticles electrodeposited on glassy carbon electrode, Anal. Biochem. 427 (2012) 26–32. https://doi.org/10.1016/j.ab.2012.04.027.

[10] A. Khan, A.A.P. Khan, A.M. Asiri, M.A. Rub, N. Azum, M.M. Rahman, S.B. Khan, S.A. Ghani, A New Trend on Biosensor for Neurotransmitter Choline/Acetylcholine—an Overview, Appl. Biochem. Biotechnol. 169 (2013) 1927–1939. https://doi.org/10.1007/s12010-013-0099-0.

[11] A. Shadlaghani, M. Farzaneh, D. Kinser, R.C. Reid, Direct Electrochemical Detection of Glutamate, Acetylcholine, Choline, and Adenosine Using Non-Enzymatic Electrodes, Sensors 19 (2019) 447. https://doi.org/10.3390/s19030447.

[12] A. Al-Shami, F. Amirghasemi, A. Soleimani, S. Khazaee Nejad, V. Ong, A. Berkmen, A. Ainla, M.P.S. Mousavi, SPOOC (Sensor for Periodic Observation of Choline): An Integrated Lab-on-a-Spoon Platform for At-Home Quantification of Choline in Infant Formula, Small 20 (2024) 2311745. https://doi.org/10.1002/smll.202311745.

[13] X. Mu, T.D. Evans, F. Zhang, ATP biosensor reveals microbial energetic dynamics and facilitates bioproduction, Nat. Commun. 15 (2024) 5299. https://doi.org/10.1038/s41467-024-49579-1.

[14] K. Phasuksom, N. Thongwattana, N. Ariyasajjamongkol, A. Sirivat, Non-enzymatic sensor based on doped polyindole/multi-walled carbon nanotube for detecting neurotransmitter acetylcholine, J. Electroanal. Chem. 964 (2024) 118337. https://doi.org/10.1016/j.jelechem.2024.118337.

[15] Varnakavi. Naresh, N. Lee, A Review on Biosensors and Recent Development of Nanostructured Materials-Enabled Biosensors, Sensors 21 (2021) 1109. https://doi.org/10.3390/s21041109.

[16] A. Villalonga, A.M. Pérez-Calabuig, R. Villalonga, Electrochemical biosensors based on nucleic acid aptamers, Anal. Bioanal. Chem. 412 (2020) 55–72. https://doi.org/10.1007/s00216-019-02226-x.

[17] E.C. Welch, J.M. Powell, T.B. Clevinger, A.E. Fairman, A. Shukla, Advances in Biosensors and Diagnostic Technologies Using Nanostructures and Nanomaterials, Adv. Funct. Mater. 31 (2021) 2104126. https://doi.org/10.1002/adfm.202104126.

[18] H.Y. Yang, Y. Li, D.S. Lee, Recent Advances of pH-Induced Charge-Convertible Polymer-Mediated Inorganic Nanoparticles for Biomedical Applications, Macromol. Rapid Commun. 41 (2020) 2000106. https://doi.org/10.1002/marc.202000106.

[19] J. An, M. Luo, M. Li, H. Cui, Y. Liu, Development of an advanced electrochemical biosensor for choline detection using MXene, MWCNT-AuNPs, and Fe3O4NPs, Microchem. J. 214 (2025) 114034. https://doi.org/10.1016/j.microc.2025.114034.

[20] M.D. Nguyen, S. Hoijang, R. Yarinia, M. Ariza Gonzalez, S. Mandal, Q.M. Tran, P. Chinwangso, T.R. Lee, Magnetic Iron Oxide Nanoparticles: Advances in Synthesis, Mechanistic Understanding, and Magnetic Property Optimization for Improved Biomedical Performance, Nanomaterials 15 (2025) 1500. https://doi.org/10.3390/nano15191500.

[21] A.O. Adeeyo, M.A. Alabi, J.A. Oyetade, T.T.I. Nkambule, B.B. Mamba, A.O. Oladipo, R. Makungo, T.A.M. Msagati, Magnetic Nanoparticles: Advances in Synthesis, Sensing, and Theragnostic Applications, Magnetochemistry 11 (2025) 9. https://doi.org/10.3390/magnetochemistry11020009.

[22] N.W. Mamdooh, I.M. Ibrahim, S.N.T. Al Rashid, Hydrothermal synthesis of spinel ferrite nanoparticles and study its effect on optical, structural and magnetic characterization, in: Baghdad, Iraq, 2025: p. 050042. https://doi.org/10.1063/5.0265654.

[23] K.K. Kadam, Synthesis Structural and Infrared Properties of Nickel Ferrite (NiFe2O4) Nanoparticles., Int. Res. J. Eng. Technol. IRJET 08 (n.d.).

[24] A.R.O. Rodrigues, I.T. Gomes, B.G. Almeida, J.P. Araújo, E.M.S. Castanheira, P.J.G. Coutinho, Magnetic liposomes based on nickel ferrite nanoparticles for biomedical applications, Phys. Chem. Chem. Phys. 17 (2015) 18011–18021. https://doi.org/10.1039/C5CP01894C.

[25] W. Ralph WG, The Chemical Catalog Company, in: Struct. Cryst., 1931.

[26] B. Sun, N. Wang, W. Hu, Synthesis of Novel $NiFe_2O_4$ /Fe_3O_4 Nanotube arrays as flexible negative electrodes for Supercapacitor Applications, IOP Conf. Ser. Earth Environ. Sci. 639 (2021) 012029. https://doi.org/10.1088/1755-1315/639/1/012029.

[27] J.A.C. De Paiva, M.P.F. Graça, J. Monteiro, M.A. Macedo, M.A. Valente, Spectroscopy studies of NiFe2O4 nanosized powders obtained using coconut water, J. Alloys Compd. 485 (2009) 637–641. https://doi.org/10.1016/j.jallcom.2009.06.052.

[28] D.R.A. El-Hafiz, M.A. Ebiad, A.A.-E. Sakr, Ultrasonic-Assisted Nano-Nickel Ferrite Spinel Synthesis for Natural Gas Reforming, J. Inorg. Organomet. Polym. Mater. 31 (2021) 292–302. https://doi.org/10.1007/s10904-020-01718-z.

[29] R.B. Kamble, V. Varade, K.P. Ramesh, V. Prasad, Domain size correlated magnetic properties and electrical impedance of size dependent nickel ferrite nanoparticles, AIP Adv. 5 (2015) 017119. https://doi.org/10.1063/1.4906101.

[30] J. Jacob, M.A. Khadar, Investigation of mixed spinel structure of nanostructured nickel ferrite, J. Appl. Phys. 107 (2010) 114310. https://doi.org/10.1063/1.3429202.

[31] Zampiva, R. Y. S., Kaufmann Jr, C. G., Venturini, J., dos Santos, L. M., Yamashita, G. H., da Cas Viegas, A., ... & Alves, A. K, Role of the fuel stoichiometry and post-treatment temperature on the spinel inversion and magnetic properties of NiFe2O4 nanoparticles produced by solution combustion synthesis, Mater. Res. Bull. 138 (n.d.).

[32] M.G. Naseri, E.B. Saion, H.A. Ahangar, M. Hashim, A.H. Shaari, Simple preparation and characterization of nickel ferrite nanocrystals by a thermal treatment method, Powder Technol. 212 (2011) 80–88. https://doi.org/10.1016/j.powtec.2011.04.033.

[33] J.L. Gunjakar, A.M. More, K.V. Gurav, C.D. Lokhande, Chemical synthesis of spinel nickel ferrite (NiFe2O4) nano-sheets, Appl. Surf. Sci. 254 (2008) 5844–5848. https://doi.org/10.1016/j.apsusc.2008.03.065.

[34] D. Guragain, B.K. Rai, S. Yoon, T.P. Poudel, S.C. Bhandari, S.R. Mishra, Effect of Terbium Ion Substitution in Inverse Spinel Nickel Ferrite: Structural and Magnetic Study, Magnetochemistry 6 (2020) 14. https://doi.org/10.3390/magnetochemistry6010014.

[35] M.I. Din, M. Javed, Z. Hussain, R. Khalid, S. Ameen, Slow Catalytic Pyrolysis of *Saccharum munja* using Bio-genically Synthesized Nickel Ferrite Nanoparticles for the Production of high yield Biofuel, Eur. J. Sustain. Dev. Res. (2020). https://doi.org/10.29333/ejosdr/7900.

[36] B.C. Reddy, H.C. Manjunatha, Y.S. Vidya, K.N. Sridhar, U.M. Pasha, L. Seenappa, C. Mahendrakumar, B. Sadashivamurthy, N. Dhananjaya, B.M. Sankarshan, S. Krishnaveni, K.V. Sathish, P.S.D. Gupta, Synthesis and characterization of multi functional nickel ferrite nano-particles for X-ray/gamma radiation shielding, display and antimicrobial applications, J. Phys. Chem. Solids 159 (2021) 110260. https://doi.org/10.1016/j.jpcs.2021.110260.

[37] S. Munir, M. Farooq Warsi, S. Zulfiqar, I. Ayman, S. Haider, I.A. Alsafari, P.O. Agboola, I. Shakir, Nickel ferrite/zinc oxide nanocomposite: Investigating the photocatalytic and antibacterial properties, J. Saudi Chem. Soc. 25 (2021) 101388. https://doi.org/10.1016/j.jscs.2021.101388.

[38] G.E. Uwaya, O.E. Fayemi, Enhanced Electrocatalytic Detection of Choline Based on CNTs and Metal Oxide Nanomaterials, Molecules 26 (2021) 6512. https://doi.org/10.3390/molecules26216512.